Space Technology 5 multipoint observations of temporal and spatial variability of field-aligned currents

G. Le,[1] Y. Wang,[2] J. A. Slavin,[3] and R. J. Strangeway[4]

Received 16 January 2009; revised 18 May 2009; accepted 26 May 2009; published 12 August 2009.

[1] Space Technology 5 (ST5) is a constellation mission consisting of three microsatellites. It provides the first multipoint magnetic field measurements in low Earth orbit, which enables us to separate spatial and temporal variations. In this paper, we present a study of the temporal variability of field-aligned currents using the ST5 data. We examine the field-aligned current observations during and after a geomagnetic storm and compare the magnetic field profiles at the three spacecraft. The multipoint data demonstrate that mesoscale current structures, commonly embedded within large-scale current sheets, are very dynamic with highly variable current density and/or polarity in ~10 min time scales. On the other hand, the data also show that the time scales for the currents to be relatively stable are ~1 min for mesoscale currents and ~10 min for large-scale currents. These temporal features are very likely associated with dynamic variations of their charge carriers (mainly electrons) as they respond to the variations of the parallel electric field in auroral acceleration region. The characteristic time scales for the temporal variability of mesoscale field-aligned currents are found to be consistent with those of auroral parallel electric field.

Citation: Le, G., Y. Wang, J. A. Slavin, and R. J. Strangeway (2009), Space Technology 5 multipoint observations of temporal and spatial variability of field-aligned currents, *J. Geophys. Res.*, *114*, A08206, doi:10.1029/2009JA014081.

1. Introduction

[2] We report the first in situ observations of temporal variability of field-aligned currents (FACs) at low altitudes in time scales of ~10 min and less using multipoint observations from Space Technology 5 (ST5) constellation. Our knowledge about properties of FACs comes mainly from single-spacecraft measurements by assuming these currents to be stationary and time independent. However, the currents are expected to be not only in motion, but also changing with time, as indicated in optical observations of aurora. Temporal variability of the field-aligned currents at time scales less than the orbit period of low Earth orbit spacecraft (~100 min) cannot be assessed using data from single spacecraft.

[3] Field-aligned currents flow along the geomagnetic lines emanating from the auroral ovals and connect the Earth's magnetosphere to the ionosphere. They are formed in response to the stress exerted on the magnetosphere by the solar wind and act as the primary mechanism for dissipating energy from the magnetosphere to the ionosphere and upper atmosphere. For nearly three decades, much work has been done to describe and classify the observed field-aligned currents. Extensive investigations using single spacecraft have produced statistical distribution of FACs in the ionosphere and shown that the auroral field-aligned currents usually appear as quasi-planar "sheets" that tend to be loosely parallel to lines of constant geomagnetic latitude [e.g., *Iijima and Potemra*, 1978]. Typically, there is a set of "Region 1" or "R1" FACs along the high-latitude edge of the auroral oval, which originate near the equatorial edge of the magnetosphere. The R1 currents flow into the ionosphere in the dawnside and out of the ionosphere in the duskside. At the lower-latitude edge of the auroral oval there is also a set of "Region 2" or "R2" FACs with polarities opposite to R1, which originate in the region where the ring current has a divergence. Other field-aligned current systems are present in the oval near local noon and midnight, the so-called "magnetic cusp" [*Erlandson et al.*, 1988] and "substorm current wedge" [*McPherron et al.*, 1973] current systems, respectively. They appear to share many characteristics of the R1 and R2 currents, but are associated with other aspects of the solar wind interaction with the geomagnetic field and the "substorms" that occur within the magnetosphere. The interaction between the solar wind and the magnetosphere is intimately controlled by the interplanetary magnetic field (IMF) and solar wind conditions [e.g., *Cowley*, 1984]. The IMF and solar wind are constantly varying, making the field-aligned current systems highly dynamic.

[4] The data from ISEE 1 and 2 magnetometers provided the first dual-point simultaneous measurements of FACs at

[1]Space Weather Laboratory, Heliophysics Science Division, NASA Goddard Space Flight Center, Greenbelt, Maryland, USA.
[2]UMBC/GEST at Space Weather Laboratory, NASA Goddard Space Flight Center, Greenbelt, Maryland, USA.
[3]Heliophysics Science Division, NASA Goddard Space Flight Center, Greenbelt, Maryland, USA.
[4]Institute of Geophysics and Planetary Physics, University of California, Los Angeles, California, USA.

Copyright 2009 by the American Geophysical Union.
0148-0227/09/2009JA014081

midaltitudes (2.4–7 R_E). *Kelly et al.* [1986] and *Chun and Russell* [1991] used these data to determine large-scale FAC properties. They found that the latitudinal speed of the current sheets ranges from 0.05 to 0.2 km/s (mapped to ionospheric altitudes) and the FACs' thickness and speed appear to change with substorm phases. Most recently, the four-spacecraft Cluster data have also been used to study FACs at midaltitudes and high altitudes (4–11 R_E) [e.g., *Cargill et al.*, 2001; *Johansson et al.*, 2004; *Draper et al.*, 2005; *Figueiredo et al.*, 2005]. The three-spacecraft ST5 mission provides the first multipoint measurements of FACs at low altitudes (~300–4500 km), which are complementary to the midaltitude and high-altitude observations.

[5] ST5 is a three-microsatellite constellation deployed into an elliptical (300 km perigee and 4500 km apogee), dawn-dusk, Sun-synchronous polar orbit from 22 March to 21 June 2006 for technology validations [*Slavin et al.*, 2008]. The three spacecraft are maintained in a string-of-pearls constellation with controlled spacing ranging from just over 5000 km down to under 50 km [see *Slavin et al.*, 2008, Figure 1]. Each spacecraft carried a miniature triaxial fluxgate magnetometer, and returned high-quality magnetic field data as the constellation flew in formation and made simultaneous multipoint measurements of the magnetic field through the Earth's dynamic ionospheric current systems. A substantial volume of magnetic field data was taken over a range of intersatellite spacing. These separations allow us to separate spatial versus temporal structures of auroral field-aligned currents over a wide range of spatial (~50–4000 km) and temporal (~5 s to 10 min) scales. Herein we report the first study on the temporal variability of FACs in these spatial and temporal scales using the multipoint ST5 data. We examine the multipoint FAC observations during a geomagnetically active period as well as a quiet period, and attempt to separate spatial and temporal variations. We evaluate time scales of temporal variations for both mesoscale and large-scale FACs. The active period we study in this paper occurs during the main phase of a geomagnetic storm when intense FAC activities are expected and also indeed observed. The quiet period occurs near the end of the recovery phase of the same geomagnetic storm.

[6] In this study, we focus on large-scale and mesoscale currents with spatial scale length greater than ~150 km. The large-scale currents generally refer to the structures which can be roughly divided into two layers with oppositely flowing R1-R2 currents. Their scale lengths are in the order of ~1000 km. The mesoscale currents here refer to the sublayers embedded within the R1-R2 layers and with scale lengths greater than ~150 km. The small-scale (~10–150 km) and microscale (~500 m to 10 km) currents are not the subject in this study.

2. Observations

[7] As the three spacecraft cross the FAC region successively along the same trajectory, their magnetic field profiles would exactly track each other except with time delays if the magnetic variations are all spatial and the FAC structures do not experience any temporal variation. Otherwise, differences in the magnetic field profiles would indicate temporal changes in the structure of the current sheets. Thus, we can study the temporal variability of the FACs using the magnetic field profiles from multiple spacecraft.

[8] We present here the observations of FACs during and after a geomagnetic storm on 13–20 April 2006 and when ST5's interspacecraft separations provide us an opportunity to study the temporal variability at both ~1 min and ~10 min time scales. Figure 1 shows the Wind interplanetary magnetic field (IMF) and solar wind speed, the *Dst* index, and the *Kp* index from 12 April to 22 April 2006. The *Dst* index at its minimum is −111 nT for the storm and the minimum *Dst* occurs around 10 UT on 14 April. The first dashed line indicates the center time of two ST5 polar cap passes near the *Dst* minimum on 14 April: a northern pass near the orbit perigee (0951–1025 UT) and a southern pass near the orbit apogee (1035–1140 UT). The second dashed line near the end of the storm recovery phase indicates the time of two ST5 polar cap passes for the quiet period on 21 April: a northern pass near the orbit perigee (1305–1345 UT) and a southern pass near the orbit apogee (1355–1455 UT).

2.1. FACs During the Active Period

[9] Figure 2 shows an overview of the two polar cap passes during the active period on 14 April 2006. The spacecraft trajectories are shown in Figure 2 (top), in which we have mapped the spacecraft positions to their ionospheric footprints at 110 km altitude along the magnetic field lines. The nested circles represent constant magnetic latitudes separated by 10° and centered at the Earth's magnetic Pole. (Note we have flipped the trajectory for the southern polar cap pass to the northern hemisphere.) The three ST5 spacecraft are named SC094, SC155 and SC224 and their trajectories are color coded in black, red and blue, respectively. The tick marks on the trajectories are separated by 10 min with color-coded time tags. During this time period, the spacecraft move across the polar cap near the dawn-dusk meridian plane: from dusk (dawn) to dawn (dusk) in the northern (southern) hemisphere. In the string-of-pearls configuration, the midspacecraft SC094 and the trailing spacecraft SC224 are close together and have a large separation from the leading spacecraft SC155. The lag time along the orbit is about 10 min from SC094 to SC155 and about 1 min from SC224 to SC094. The spacecraft spacing is ~5331 (~3564) km from SC155 to SC094 and ~531 (~368) km between SC094 and SC224 over the northern (southern) polar cap. Thus, the observations from this pass allow us to evaluate the FAC variability at these two temporal and spatial scales.

[10] Figure 2 (bottom) shows an overview of ST5 magnetic field variations generated by the field-aligned currents during these two passes, including the three components of the magnetic field residual vector (data with the internal IGRF model magnetic field removed) in the solar magnetic (SM) coordinate system, as well as the residual of the magnetic field strength. Since this is an active period with a strongly southward IMF, we have observed in the data strong FAC activities in the auroral region as expected. The data from the three spacecraft are color coded corresponding to those in the spacecraft orbits, but the labels for the spacecraft positions (altitudes, magnetic latitudes and magnetic local times) on the bottom of Figures 2 (bottom left) and 2 (bottom right) are for

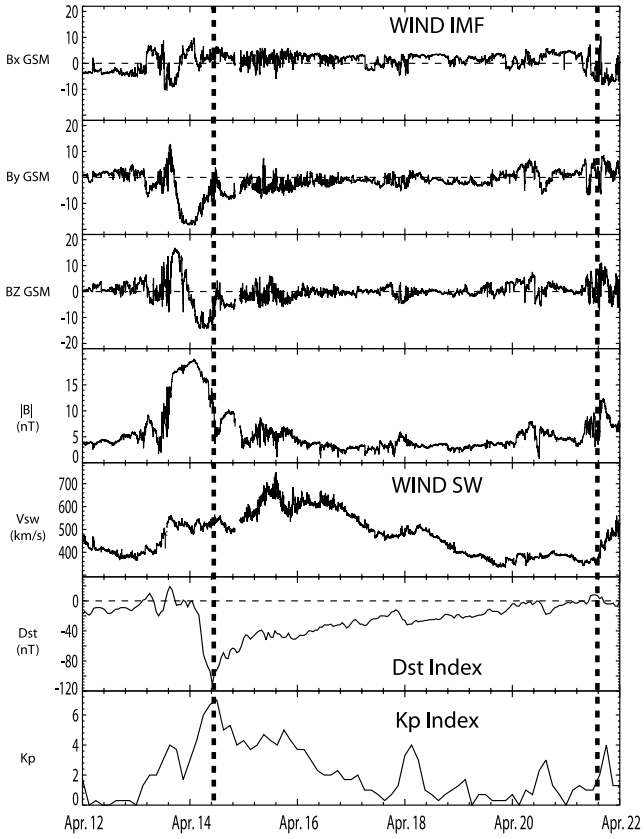

Figure 1. The Wind interplanetary magnetic field (IMF) and solar wind speed, the *Dst* index, and the *Kp* index from 12 April to 22 April 2006. The dashed lines indicate the times for a northern polar cap pass and a southern polar cap pass presented in the paper.

midspacecraft SC094 only. The magnetic field data shown in Figure 2 all have a time resolution of 1 s, which are spin-averaged data with overlapped averaging windows. The spin periods are about 3 s and are slightly different for the three spacecraft.

[11] Since FACs flow along the background magnetic field direction, their magnetic field perturbations are transverse to the background field (as FACs are carried by shear Alfven waves). In the high field region where the Earth's magnetic field (~10,000 to 40,000 nT) is much larger than the perturbation field (~10 to 1000 nT), the presence of FACs twists the field line directions without changing the field strength. Thus, the signatures of FACs can be seen only in the components of the magnetic field data but not in the magnetic field strength (similar to those of transverse waves). We do see some perturbations of the magnetic field strength associated with FACs in the passes near the orbit perigee with altitudes less than ~1000 km, such as the case in Figure 2 (bottom left). But these perturbations are generated by the ionospheric horizontal currents (mainly the Hall currents), and are not the subject of this paper. As the altitude increases, magnetic perturbations of ionospheric currents decrease and eventually become undetectable, as in the case in Figure 2 (bottom right).

[12] In Figure 2, the encounters of field-aligned currents are evident by perturbations of magnetic field components as large as ~1000 nT, and occur two times in each pass, once in the dawn side and once in the dusk side. In each encounter, the FAC signatures are first seen by the leading spacecraft SC155 (red), and then by the midspacecraft SC094 (black), and finally by the trailing spacecraft SC224 (blue). The magnetic field profiles at the three spacecraft enable us to distinguish spatial and temporal variations.

[13] Traditionally, it is common to treat the large-scale FAC current sheet as an infinite planar sheet locally aligned with the circle of constant magnetic latitude (L shell alignment) in analyzing the magnetic field data. Under the infinite current sheet approximation, if the spacecraft crosses the current sheet with a large attack angle (the angle between the orbit track and the current plane), the FAC signature appears to be a magnetic field variation only in the azimuthal component perpendicular to the magnetic meridional plane and along the east–west direction. Then the current density can be calculated from the gradient of this azimuthal component by assuming the magnetic field variation is completely due to the spatial variation when crossing the current sheet. *Fung and Hoffman* [1992] evaluated the finite geometry effects of the field-aligned current sheet and concluded that the infinite current sheet assumption works well except when the spacecraft crosses the finite length current sheet near the end. Near the end of the finite current sheet, the magnetic field perturbation will not be confined to one azimuthal component. Instead, the FAC magnetic field signatures will appear in both the east–west azimuthal component and the north–south component. Furthermore, there are commonly mesoscale and small-scale currents embedded within large-scale FACs [e.g., *Fukunishi et al.*, 1991; *Hoffman et al.*, 1994; *Higuchi and Ohtani*, 2000; *Neubert and Christiansen*, 2003]. Previous studies have indicated these currents generally consist of filamentary or finite current segments and cannot be treated as large-scale sheet currents.

[14] Thus, our first analysis to the magnetic field data is to evaluate the infinite current sheet assumption for the large-scale currents and how close the current sheet is aligned with the L shell. We first perform the Minimum Variance Analysis (MVA) [*Sonnerup and Cahill*, 1967] to the magnetic field variations in the FAC region using the low-pass-filtered data (so that the minimum variance coordinates are determined by large-scale currents only). The coordinate system determined by the MVA are denoted as ($\boldsymbol{i}$, $\boldsymbol{j}$, $\boldsymbol{k}$), where $\boldsymbol{i}$, $\boldsymbol{j}$, and $\boldsymbol{k}$ are the maximum, intermediate, and minimum variance directions, respectively. For FACs, $\boldsymbol{k}$ is also the field-aligned direction, and $\boldsymbol{i}$ and $\boldsymbol{j}$ are the two directions transverse to the magnetic field. If the magnetic field variations are mainly seen in the $\boldsymbol{i}$ direction, the infinite current sheet would be a good approximation, and the current sheet normal direction would be along the $\boldsymbol{j}$ direction. Otherwise, the spacecraft is close to the end of a finite current sheet where the magnetic field variations would be seen in both $\boldsymbol{i}$ and $\boldsymbol{j}$ directions.

[15] Here we use the data from the northern polar cap pass to describe the details of our data analysis, and the same techniques will be applied to other intervals presented in this paper. Figure 3 shows the FAC magnetic field variations displayed in the MVA coordinate system for the northern polar cap pass, with the duskside FACs on the left and dawnside FACs on the right. In performing the MVA to

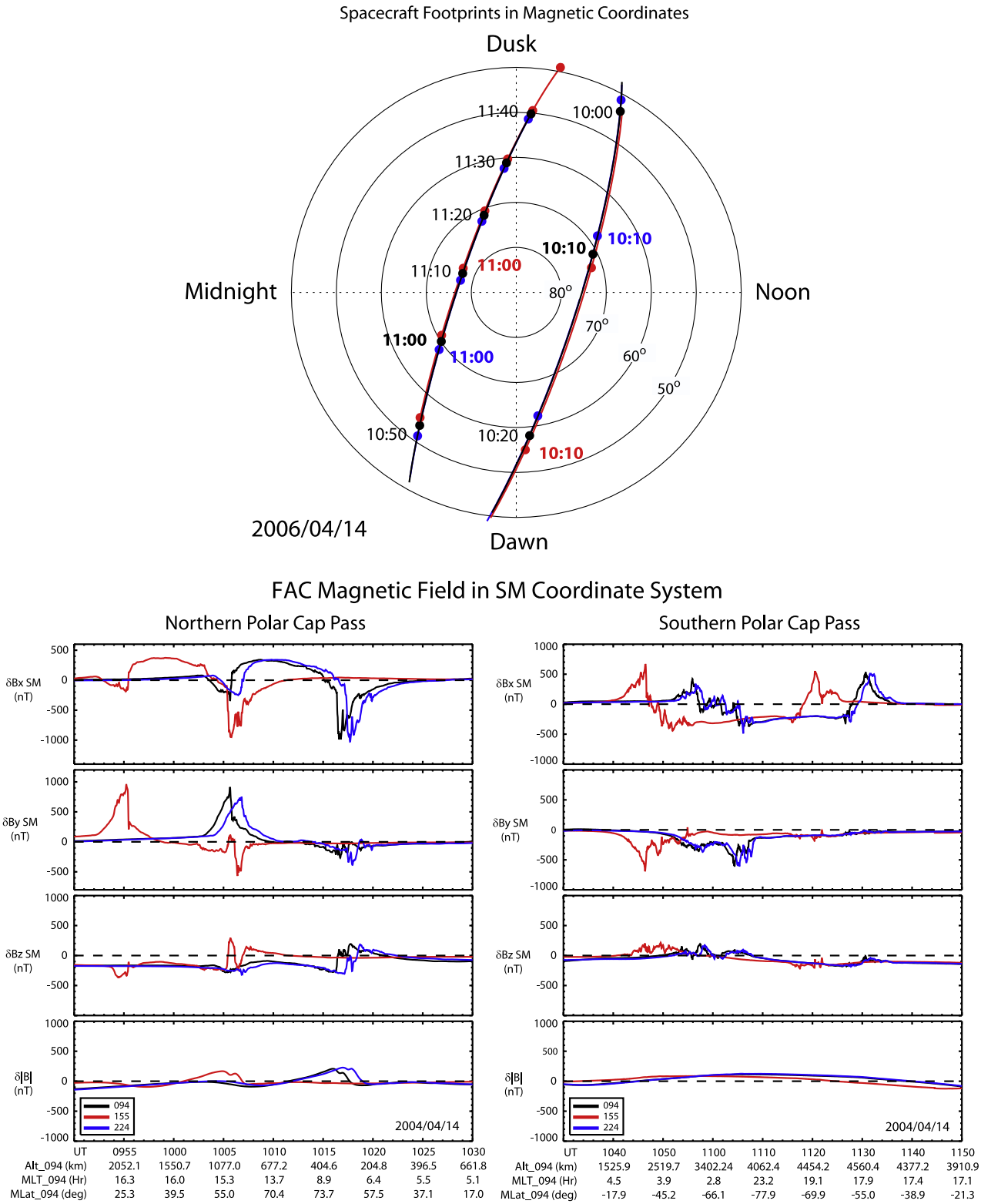

Figure 2. (top) The spacecraft ionospheric footprints at 110 km altitude for the two polar cap passes during the active period on 14 April 2006. The footprints for the southern pass have been flipped to the northern polar cap. The nested circles represent constant magnetic latitudes separated by 10° and centered at the Earth's magnetic Pole. (bottom) Overview of ST5 magnetic field variations generated by the field-aligned currents on 14 April 2006. The three components of the magnetic field residual vector (data with the internal IGRF model magnetic field removed) are shown in SM coordinates. The labels for the spacecraft positions (altitudes, magnetic latitudes, and magnetic local times) on the bottom are for midspacecraft SC094 (black) only.

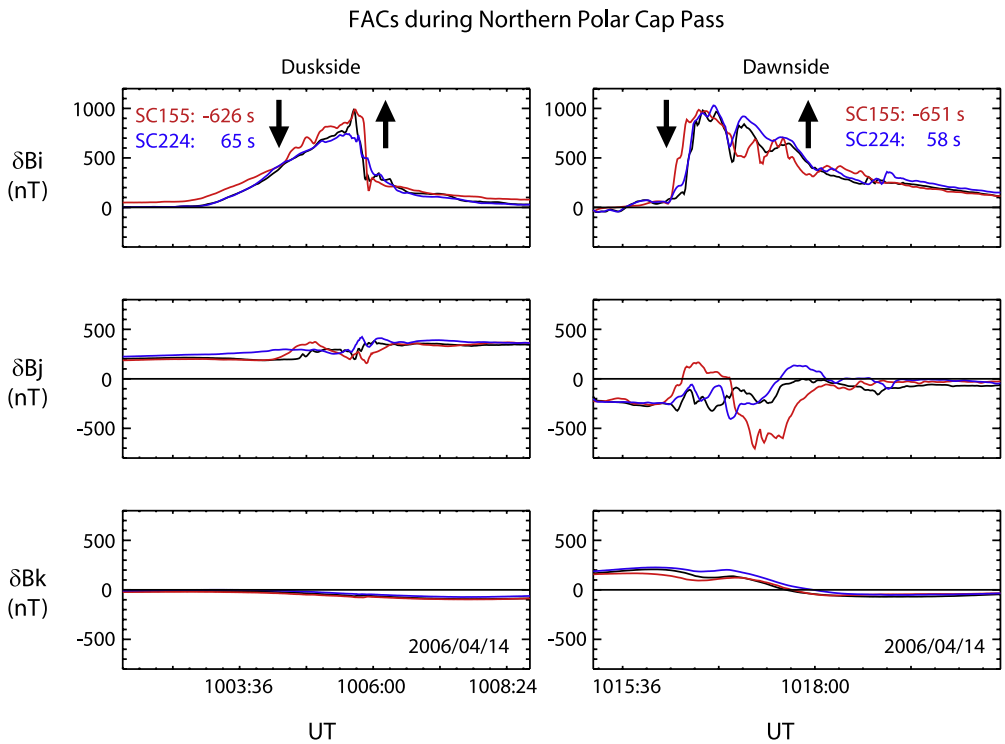

Figure 3. The FAC magnetic field variations displayed in the MVA coordinate system for the northern polar cap pass during the active period. The magnetic field data from the leading (red) and trailing (blue) spacecraft have been time-shifted by the amount listed in the top to line up with the large-scale current structures of the midspacecraft (black). The arrows indicate the general direction of the large-scale currents with a downward arrow for currents flowing into the ionosphere and an upward arrow for currents flowing out of the ionosphere.

the data, we have used the smoothed data so that the MVA coordinate system is determined by variations in spatial scale greater than ~150 km. In Figure 3, the data from SC155 and SC224 are time shifted by the amount determined from the cross-correlation analysis of large-scale current structures in the maximum variance component δB_i; the time labels on the bottom of the horizontal axis are for SC094 only.

[16] For the duskside FACs in Figure 3, the large-scale magnetic field variations are mainly in the δB_i component, and the δB_j component contains mainly mesoscale variations at all three spacecraft. The ratios of the maximum variance eigen-value to the intermediate variance eigen-value, e_i/e_j, are listed in Table 1. They are 13.1, 12.8, and 15.5 for SC094, SC155, and SC224, respectively. These observations indicate that the infinite current sheet approximation applies to the large-scale FACs observed here. Since the mesoscale variations are seen in both δB_i and δB_j, the mesoscale currents are filamentary, and cannot be treated as an infinite sheet current. To examine the L shell alignment of the large-scale current sheet, we also list the azimuthal angle of the $\boldsymbol{j}$ direction (the current sheet normal direction defined by MVA) from the magnetic meridional plane in Table 1. This angle will be 0 if the current sheet has a perfect L shell alignment. For the duskside FACs, this angle is very small at all three spacecraft, indicating the large-scale current sheet is closely aligned to the L shell in this case.

[17] For the dawnside FACs in Figure 3 (right), the large-scale FACs still appear mainly in the δB_i component, but there are significant mesoscale variations in the δB_j component. The large-scale current sheet is not as closely aligned to the L shell as in the previous case since the azimuthal angle of the $\boldsymbol{j}$ direction becomes much larger (Table 1). The eigen-value ratio e_i/e_j (Table 1) also becomes smaller, especially at SC155 where the magnitude of mesoscale variations in δB_j is comparable to that of large-scale variations in δB_i. It is possible that the large δB_j variations are caused by mesoscale currents that cannot be described as planar current sheets. It is also possible that SC155 crosses the edge of the large-scale current sheets, followed by SC094 and SC224 further into the current sheets. Here it is difficult to separate large-scale and mesoscale currents unambiguously.

[18] The time-shifted magnetic field data from the three spacecraft in Figure 3 enable us to distinguish the FAC's temporal variations from spatial ones. After lining up the large-scale spatial structures at the three spacecraft, the characteristics of FACs temporal variations are very evident for the both FAC intervals. First of all, large-scale currents shown mainly in the top plots are relatively stable in time scales of ~10 min. The duration and magnitude of the overall δB_i variations maintain the similar values at the three spacecraft. However, the mesoscale structures within the large-scale currents show significant changes in the same time scales. The magnetic field variations of the mesoscale currents are in both δB_i and δB_j components. Comparing the observations ~10 min apart between the leading and the midspacecraft or trailing spacecraft (red versus black/blue

Table 1. Results of Minimum Variance Analysis

FACs	e_i/e_j Ratio	Azimuthal Angle of $\boldsymbol{j}$ Axis	Attack Angle	S/C Velocity (km/s)
		14 April 2006 (Active Period)		
North/dusk (Figure 3)	SC094: 13.1	SC094: 5°	45°	$v_i = -5.223$
	SC155: 12.8	SC155: 1°		$v_j = -5.302$
	SC224: 15.5	SC224: 8°		
North/dawn (Figure 3)	SC094: 9.8	SC094: 41°	77°	$v_i = 1.951$
	SC155: 2.2	SC155: 39°		$v_j = -8.305$
	SC224: 6.0	SC224: 29°		
South/dawn (Figure 4)	SC094: 3.1	SC094: 25°	66°	$v_i = -2.429$
	SC155: 7.0	SC155: 2°		$v_j = 5.574$
	SC224: 2.3	SC224: 36°		
South/dusk (Figure 4)	SC094: 97.8	SC094: 21°	61°	$v_i = -2.456$
	SC155: 61.2	SC155: 9°		$v_j = 4.520$
	SC224: 398.5	SC224: 22°		
		21 April 2006 (Quiet Period)		
North/dawn (Figure 6)	SC094: 25.9	SC094: 17°	22°	$v_i = 7.934$
	SC155: 7.5	SC155: 15°		$v_j = -3.276$
	SC224: 15.2	SC224: 16°		
South/dawn (Figure 7)	SC094: 38.8	SC094: 6°	73°	$v_i = -1.776$
	SC155: 75.9	SC155: 9°		$v_j = 5.949$
	SC224: 30.5	SC224: 5°		
South/dusk (Figure 7)	SC094: 46.8	SC094: 2°	81°	$v_i = 0.786$
	SC155: 33.2	SC155: 6°		$v_j = 5.122$
	SC224: 62.8	SC224: 5°		

traces), the mesoscale structures at SC155 exhibit the largest differences from those of SC094 and SC224. We can observe changes in magnitude, polarity, as well as locations for the mesoscale currents.

[19] Figure 4 is in the same format as Figure 3 but for the FACs observed during the southern polar cap pass. Their properties from the MVA are also listed in Table 1. For the dawnside FACs (Figure 4, left), the large-scale currents are not very planar, as we can see large variations in δB_j component (small ratio of e_i/e_j). On the other hand, the large-scale duskside FACs (Figure 4, right) appear to be a very planar current sheet with large e_i/e_j ratio. The observed current sheet is not perfectly aligned with the L shell as the azimuthal angle of the $\boldsymbol{j}$ direction is greater than 10° in this case.

[20] Again, the mesoscale currents show significant temporal variations in ~10 min time scales. In particular for the dawnside FACs, the mesoscale currents observed by the

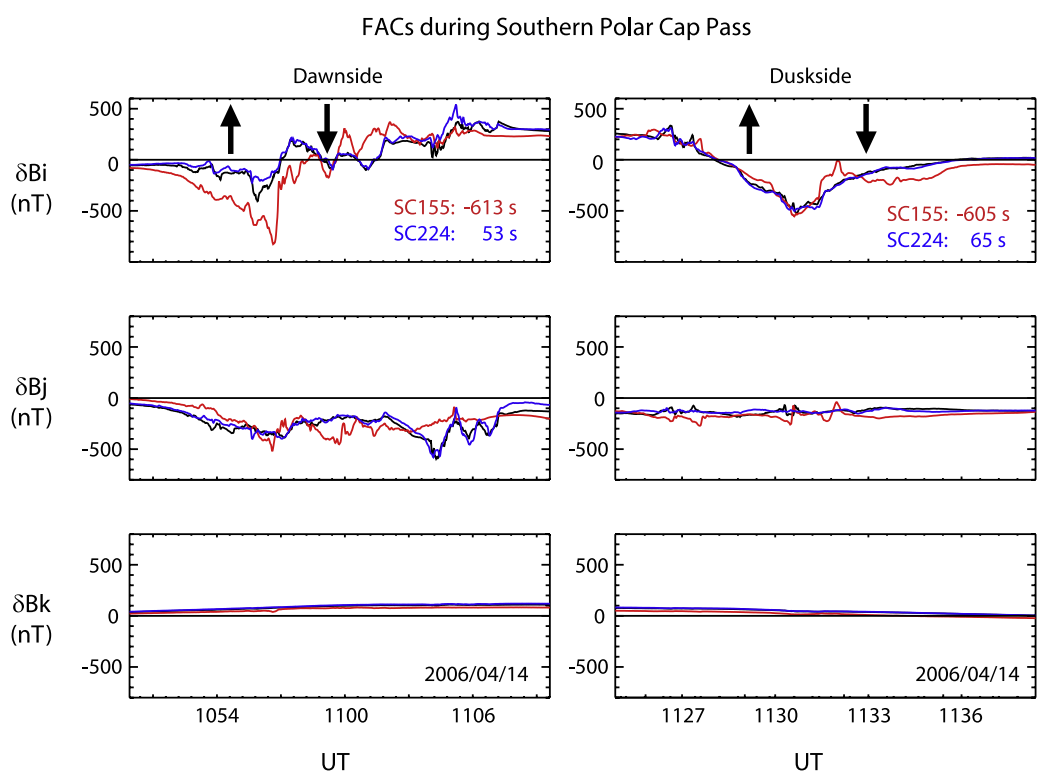

Figure 4. The FAC magnetic field variations displayed in the MVA coordinate system for the southern polar cap pass during the active period. It is in the same format as Figure 3.

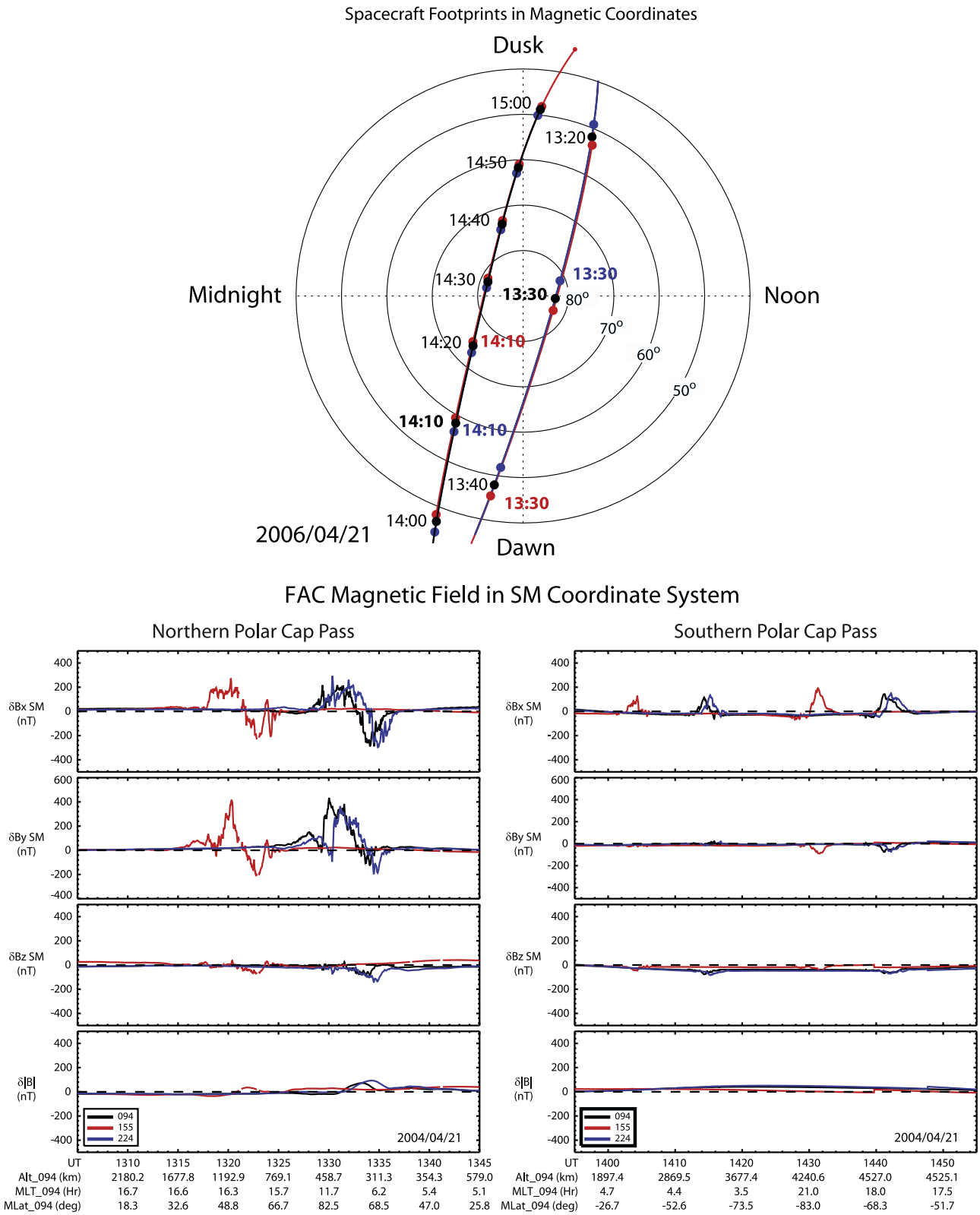

Figure 5. (top) The spacecraft ionospheric footprints at 110 km altitude for the two polar cap passes during the quiet period on 21 April 2006. (bottom) Overview of the ST5 observations of the FAC magnetic field variations. It is in the same format as Figure 2.

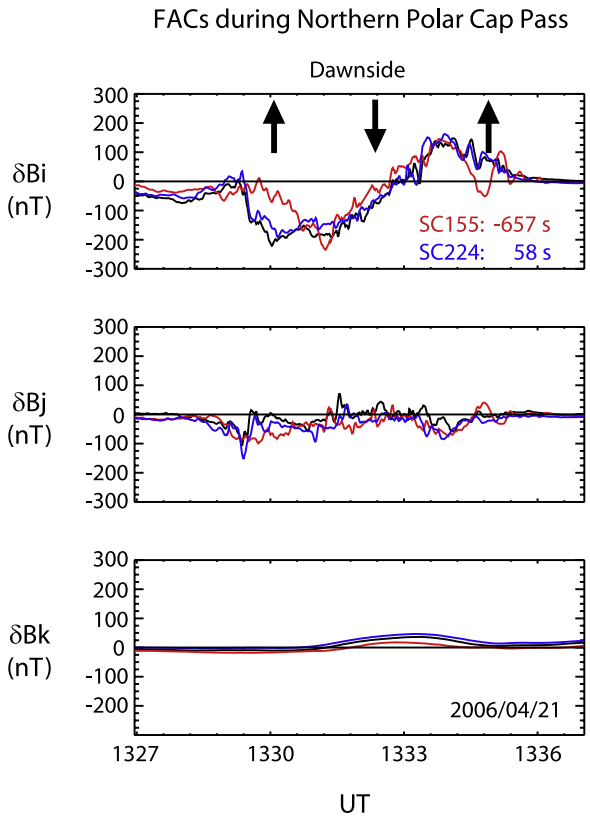

Figure 6. The FAC magnetic field variations displayed in the MVA coordinate system for the northern polar cap pass during the quiet period. It is in the same format as Figure 3.

leading spacecraft (red traces) are quite different from those at the other two spacecraft (black/blue traces). Before ~1058 UT, the mesoscale currents have clearly weakened after ~10 min, but the currents after 1058 UT has intensified over the same 10 min time scale. For the duskside FACs, the largest temporal variations occur within the lower-latitude portion of the current sheet, where a sublayer of currents at ~1132 UT observed by SC155 appears to have smoothed out after ~10 min. The currents observed ~1 min apart at SC094 and SC224, on the other hand, are very similar except at very fine scales.

2.2. FACs During the Quiet Period

[21] Figure 5 shows an overview of the two polar cap passes during the quiet period on 21 April 2006, when the geomagnetic storm has nearly fully recovered (see Figure 1). It is in the same format as Figure 2. The spacecraft spacing is ~5407 (~3534) km from SC155 to SC094 and ~501 (~335) km between SC094 and SC224 over the northern (southern) polar cap. Comparing to the case of the active period in Figure 2, the FACs during the quiet time are clearly much weaker, as evident by the smaller magnitude of the magnetic field variations. In addition, there is only one encounter with FACs during the northern polar cap pass. The FACs are not observed in the duskside during the pass. The signatures of the FACs appear during ~1328–1336 UT (for SC094), when the spacecraft are mainly in the prenoon sector moving toward the dawn.

[22] Figure 6 shows the time-shifted magnetic field variations displayed in the MVA coordinate system for the FACs in prenoon sector during the northern polar cap pass in the same format of Figure 3. The properties of the FACs from the MVA are listed in Table 1. The attack angles listed

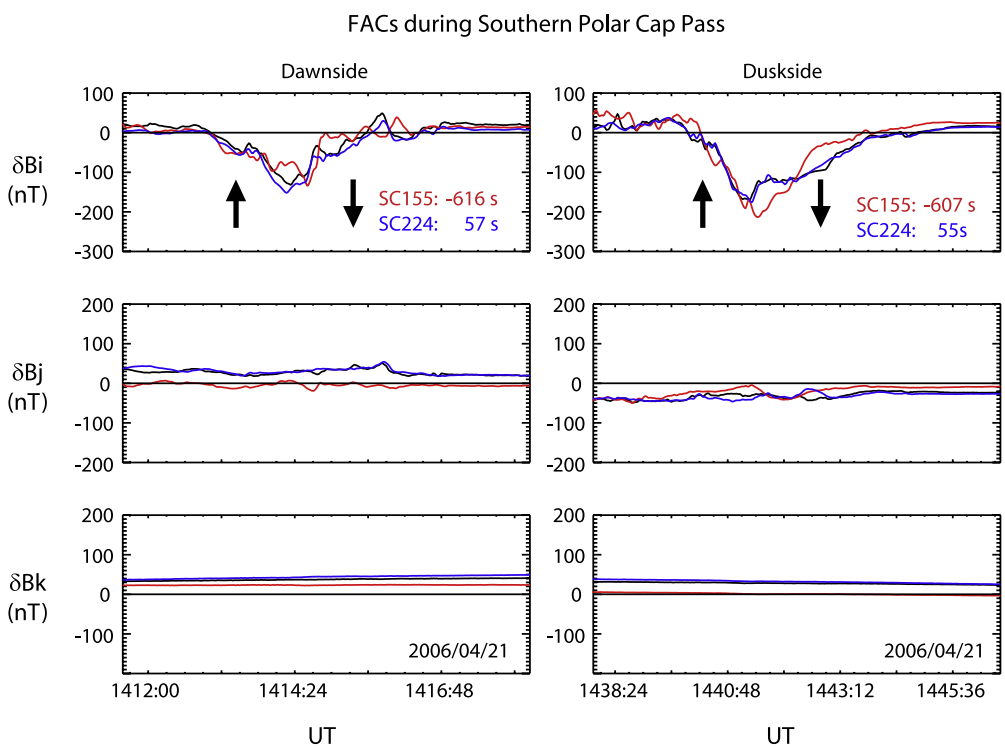

Figure 7. The FAC magnetic field variations displayed in the MVA coordinate system for the southern polar cap pass during the quiet period. It is in the same format as Figure 3.

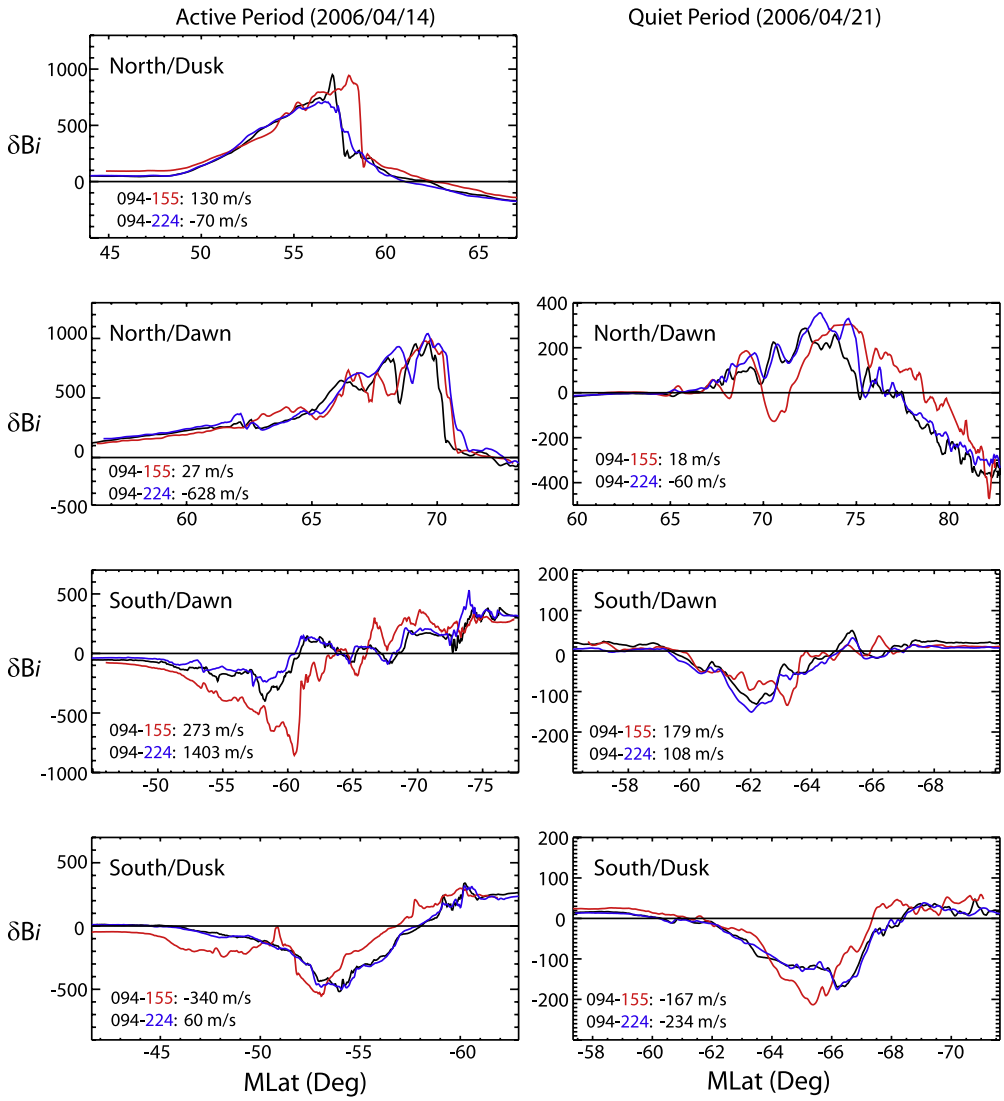

Figure 8. Profiles of the magnetic field variations in the maximum variance component as a function of the spacecraft geomagnetic latitudes, showing the motion of the large-scale current sheet as seen by the three spacecraft.

in Table 1 are determined using data from the reference spacecraft SC094. Although the spacecraft cross the FACs with a very small attack angle from the current layers (the attack angle is 22°), the MVA still yields reasonably large ratio of e_i/e_j, indicating a sheet-like current structure at the large scale. Comparing to the active period cases, the MVA also yield very agreeable $\boldsymbol{j}$ directions (the current sheet normal directions) among the three spacecraft, because the large-scale magnetic field variations appear to be less dynamic and more coherent at the three spacecraft. Here the angle between the $\boldsymbol{j}$ direction and the azimuthal direction is not a good measure of the L shell alignment of the current sheet as in other cases owing to the relatively large azimuthal extent of the current sheet observation (since the azimuthal direction has changed significantly during the FAC interval). Similar to the observations during the active period, the temporal variations of the FACs during the quiet period also occur mainly for mesoscale currents. In ~10 min time scale, the mesoscale structures have changed markedly.

[23] Figure 7 shows the time-shifted magnetic field variations in the MVA coordinate system for the FACs during the southern polar cap pass. During this pass, the spacecraft observe the FACs both in the dawn and dusk. The FACs are fairly week in comparison with those during the active period. But in both locations, the L shell aligned infinite current sheet approximation works remarkably well at all three spacecraft. The *ei*/*ej* ratios from the MVA (Table 1) are largest among all the FAC cases; and the azimuthal angles of the $\boldsymbol{j}$ direction are very small and agreeable among the three spacecraft. For these two cases, the attack angles of the spacecraft crossing the current sheets are also very large, good for the determination of the current properties using the magnetic field variations.

[24] In Figure 7, the magnetic field profiles of the FACs exhibit the similar characteristics in their temporal variations. Again, the large-scale structures of the FACs, which are only shown in the δB_i component, are very stable over the ~10 min time scale. But the mesoscale structures, which appear in both the δB_i and δB_j components, are quite

variable in ~10 min time scales, as the magnetic field variations at the leading spacecraft (red traces) are markedly different from the midspacecraft and trailing spacecraft (black/blue traces).

2.3. Motion of Large-Scale Current Sheets

[25] The multipoint observations also allow us to determine if and how the FACs move in space. One way to visualize the current sheet motion is to display the three magnetic field profiles as a function of the spacecraft latitudes, as the FAC current sheet moves mainly latitudinally. Figure 8 shows the magnetic field variations in the maximum variance component δB_i as a function of spacecraft latitudes for all the FAC intervals presented above. In Figure 8, the poleward direction is always to the right, and the equatorward to the left. Each plot illustrates how much the large-scale current sheet has moved in magnetic latitudes when the three ST5 spacecraft see them sequentially. In all cases, we observe the motion of the large-scale current sheets, either poleward or equatorward, especially between the leading spacecraft (red traces) and the midspacecraft/trailing spacecraft (black/blue traces).

[26] Figure 8 also shows that the current sheet motion also exhibits rapid temporal variations. For example, for the FACs observed at dusk in the northern hemisphere during active period (Figure 8, top left), the large-scale currents appear to be moving equatorward during the observing period. They are first observed by SC155 at higher latitudes, and subsequently at lower latitudes when encountered by the other two spacecraft. Similarly, we can determine that the FACs observed at dusk in the southern hemisphere during the active period (Figure 8, bottom left) move poleward during the observing period, as they are first observed at lower latitude and subsequently at higher latitudes. The FACs during the other two active intervals (Figure 8 (left), second and third panels) show more complicated patterns. For FACs at dawn in the northern hemisphere (Figure 8 (left), second panel), the large-scale currents show both equatorward (from SC155 to SC094) and polarward (from SC094 to SC224) motion during the ~10 min interval. For FACs at dawn in the southern hemisphere (Figure 8 (left), third panel), the low-latitude portion of the currents clearly show equatorward motion, but we are not able to determine the motion of the high-latitude portion of the currents owing to their large temporal variations in this time period. For the FACs observed during the quiet period, we observe the similar latitudinal motion of the current sheets.

[27] We can calculate the velocity of the large-scale current sheet $v_j(FAC)$, which is the velocity along the current sheet normal $\boldsymbol{j}$ direction from SC094, using the spacecraft position and timing information observed here. For example, using the data from SC094-SC155 pair, we have determined the time delay δt for the large-scale current structure based on cross-correlation analysis as shown in Figures 3, 4, 6, and 7. (Note it may be different from time delays of mesoscale structures.) If we select a single key data point at time t in SC094 data, the corresponding key point in SC155 data is at time $t + \delta t$. We use the midpoint of the large-scale currents as the key point in the calculation. Using the spacecraft positions for SC094 at time t and SC155 at time $t + \delta t$, we can calculate the large-scale FAC velocity along the current sheet normal direction (which is mainly in the latitudinal direction). The errors in this calculation are discussed by *Slavin et al.* [2008] and *Wang et al.* [2009]. Using data from SC155 and SC094 pair which are ~10 min apart, the calculated velocities represent the average over ~10 min periods. If we use the closely spaced spacecraft pair, SC094 and SC224, the calculated FAC velocities more closely represent the instantaneous value. The calculated velocities $v_j(FAC)$ are listed in Figure 8, where positive and negative values indicate equatorward and poleward motion, respectively. These observations show that the velocities of FACs are quite variable over ~10 min time scale, as the average velocity is quite different from the instantaneous velocity. But all of them remain in the range $\leq$1 km/s, comparable to the inferred velocities at the ionosphere from previous observations at midaltitudes and high altitudes [*Kelly et al.*, 1986; *Chun and Russell*, 1991]. At the low altitudes of ST5 orbit, they are much smaller than the spacecraft velocity listed in Table 1. In these examples, the ratio of $v_j(FAC)/v_j(S/C)$ are typically less than 10%, but can reach up to 25%. At midaltitudes and high altitudes where the spacecraft velocity gets smaller, we expect the overall ratio will increase [*Lockwood et al.*, 2001]. A statistical study of the large-scale current sheet velocity using ST5 multipoint observations has been reported by *Wang et al.* [2009]. Their results show that the current sheets tend to move faster when the level of geomagnetic activities increases.

2.4. Current Sheet Thickness and Current Density

[28] Previously, we have to make the assumption of stationary current sheets, or $v_j(FAC) = 0$, in calculating the thickness of the current sheet and the current density using data from single spacecraft. The $v_j(FAC)/v_j(S/C)$ ratio represents the error in the calculations under this assumption. Multispacecraft observations allow us to determine the FAC current sheet thickness and the current density more accurately. Here, we can determine the relative velocity between the FACs and the spacecraft using the average velocity of the FACs obtained above, and transform the magnetic field temporal profile, δB versus t, into the spatial profile along the current sheet normal, δB versus x_j, where $x_j = v_j(t - t_o)$, v_j is the relative velocity between the FAC current sheet and the spacecraft along the $\boldsymbol{j}$ direction $v_j = v_j(S/C) - v_j(FAC)$, and t_o is an arbitrary starting time (since we are only interested in the thickness). The field-aligned current density j_k can be calculated as $j_k = (1/\mu_o)[\partial(\delta B_i)/\partial x_j - \partial(\delta B_j)/\partial x_i]$, where x_i is the spacecraft displacement within the current sheet along the $\boldsymbol{i}$ direction $x_i = v_i(S/C)\cdot(t-t_o)$. Here we still use the single-spacecraft data to deduce the current density as in the calculations in previous studies. But in most previous works, the FACs are assumed to be an infinite current sheet and the magnetic field variations are only in the δB_i component. The difference here is that the magnetic field variations in the $\boldsymbol{j}$ direction are also considered as we have demonstrated that the mesoscale currents cannot be treated as infinite current sheets. In our calculations, the field-aligned current density j_k contains two terms: $j_k = j_k(B_i) + j_k(B_j)$, where $j_k(B_i) = (1/\mu_o)[\partial(\delta B_i)/\partial x_j]$ and $j_k(B_j) = -(1/\mu_o)[\partial(\delta B_j)/\partial x_i]$. Since the large-scale FACs are mainly in δB_i but mesoscale FACs are in both δB_i and δB_j, the first term $j_k(B_i)$ contains

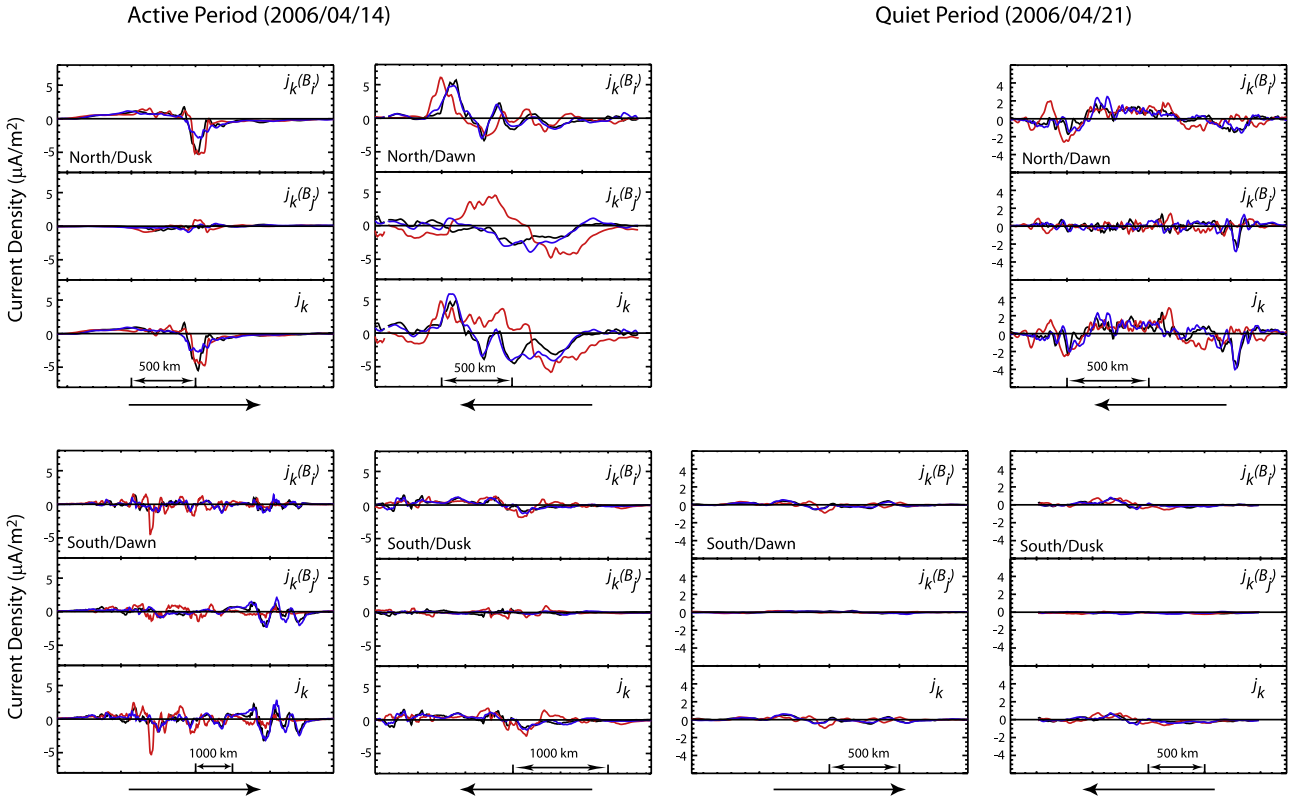

Figure 9. The deduced FAC current density profiles at the three spacecraft, which are time-shifted to line up the large-scale structures. In each plot, $j_k(B_i)$ is the current density term calculated from the derivatives of dB_i along the $\boldsymbol{j}$ direction, $j_k(B_j)$ is from the derivatives of dB_j along the $\boldsymbol{i}$ direction, and j_k is the sum of the two terms, or the total FAC current density.

both large-scale and mesoscale FACs, and the second term $j_k(B_j)$ contains mainly mesoscale FACs.

[29] Figure 9 shows the spatial profile of the current density across the current sheets for all the FAC intervals presented in this paper. In Figure 9, the spatial profiles from the three spacecraft have been time-shifted so that the large-scale current structures are lined up in space. We have also smoothed the current density profiles by applying a running average so that the spatial resolution is ~50 km. In each plot, we show $j_k(B_i)$, $j_k(B_j)$and j_k from top to bottom. The positive (negative) density is for currents flowing in the same (opposite) direction of the magnetic field. The horizontal axis is only labeled with spatial scale along the normal direction of the large-scale current sheet. The arrow at the bottom of each profile shows the poleward direction across the large-scale current sheet.

[30] The FACs can be loosely divided into two large-scale regions (>~1000 km) with opposite net currents. The spatial scales for these large-scale regions are in the order of ~1000–4000 km. There are many mesoscale structures (~100–500 km) with currents flowing upward or downward, embedded within the large-scale current sheets. During the active period, the mesoscale currents are at times more intense than the large-scale currents. It is evident that the large-scale current sheets as seen by the three spacecraft are very similar in their spatial extent, but the mesoscale structures within the large-scale current sheets have shown many temporal variations. The temporal variations can be in the form of changing current density, changing current polarity, or location changes. The mesoscale current structures observed by SC155 are quite different from those by SC094 and SC224 at ~10 min later, but the current structures by SC094 and SC224 at ~1 min apart are similar. Thus, for the events presented here, the time scales for the decay and intensification of mesoscale current structures appear to be in the order of ~10 min. These examples have clearly shown that the temporal variations of the magnetic field are caused by the variations of mesoscale currents.

3. Summary and Discussions

[31] ST5 provides the first multipoint measurements of the magnetic field in the field-aligned current region at low altitudes, which enables us to evaluate the FACs' temporal variability. In the examples presented in this paper, we have provided the first direct observations of rapid temporal variations of mesoscale field-aligned currents at low altitudes. Although the FACs examples presented in this report occur during and after a geomagnetic storm, ST5 data show that temporal variability in ~10 min time scales is common for mesoscale current structures at all levels of geomagnetic activities. The temporal features in such time scales can be inferred from observations of ionospheric convection or optical observations of mesoscale auroral structures such as auroral arcs [e.g., *Marchaudon et al.*, 2004]. Although previous observations have revealed that mesoscale current structures are commonly embedded within large-scale

current sheets during disturbed time [*Hoffman et al.*, 1985], direct observations of their temporal variability in ~10 min time scales are not possible with single-spacecraft data. But temporal variations in ~10 min time scales fall right within the bandwidth of the ionospheric variability as previous observations show that majority of the temporal variations in ionospheric convection has periods less than 1 h [*Crowley and Hackert*, 2001]. With the single-spacecraft observations, one can only systematically study the temporal variations with time scale in the order of 1 h, or one spacecraft orbit. Thus, multiple spacecraft observations such as the ones we present in this paper are necessary to characterize the temporal variability of field-aligned currents and associated phenomena.

[32] In this paper, we present an event study of the FAC temporal variability using multipoint ST5 magnetic field data. We examine the ST5 observations in an active period during a geomagnetic storm and compare them with those observed when the geomagnetic storm has fully recovered. We summarize these observations as follows:

[33] 1. By performing the minimum variance analysis to the FAC magnetic field data, we find that the large-scale FAC's magnetic signatures can be modeled as those of infinite current sheets as they are mainly confined to one single component δB_i, but the orientation of the large-scale current sheet is more likely to be aligned with the L shell during the quiet time (Table 1). During the active period, the observed current sheet orientation can be as much as ~40° off the L shell. The differences among the current sheet orientations as seen by the three spacecraft are also much larger for the active period than the quiet period, indicating the FACs are more dynamic during the active period.

[34] 2. The magnetic field variations from the mesoscale currents appear in both δB_i and δB_j components, indicating that they are generally in the form of current filaments instead of infinite sheet currents. The mesoscale currents are more prominent during the active period, as the variations in δB_j become comparable to those in δB_i in some cases during the active period.

[35] 3. The mesoscale current structures which are embedded in the large-scale current sheet exhibit significant temporal changes. The temporal variations can be in the form of changing current density, changing current polarity, or location changes. The time scale of such temporal variability is in the order of ~10 min. On the other hand, the data also show that the time scales for the currents to be relatively stable are ~1 min for mesoscale currents and at least ~10 min for large-scale current sheets.

[36] 4. The multipoint data also demonstrate the motion of the current sheets and the temporal variations of the velocity of the current sheets, especially during the active period. At low altitude, the current sheet velocity is typically smaller than 1 km/s and much smaller than the spacecraft velocity. But the effect of the current sheet motion to the calculation of the current properties is expected to increase at higher altitudes as the current sheet will move faster and the spacecraft slower as the altitude increases.

[37] Field-aligned currents are inherently very dynamic and reflect temporal variations in the coupled magnetosphere-ionosphere system. Field-aligned currents are established during the solar wind–magnetosphere coupling: electric fields produced at the magnetosphere and imposed on the ionosphere drive currents perpendicular to the magnetic field in both regions; field-aligned currents must flow because of gradients in these currents so that they reach an agreement between the magnetosphere and ionosphere, and together form a closed current system. Temporal variations in any part of the closely coupled system will result in corresponding self-consistent adjustment of FACs. For example, any change in the electric field will change field-aligned currents so that the agreement and closed current loop are maintained. Electromagnetic energy carried by FACs are eventually deposited in the high-latitude thermosphere-ionosphere system as Joule heating, which causes changes of ionosphere and thermosphere in global scale, such as ion outflows [*Chappell et al.*, 1987; *Moore*, 1991], and changes in *F* region density [*Emery et al.*, 1999] and thermospheric composition and neutral wind [*Buonsanto*, 1999]. Meanwhile, changes in ionospheric conductivity and neutral wind also modify the ionospheric horizontal currents and field-aligned currents, which in turn modify the electric field and ionospheric conductivity further. Thus, studying temporal variations of field-aligned currents helps us understand the dynamic nature of the coupled magnetosphere-ionosphere system.

[38] Previous studies have shown that the charge carriers of mesoscale FACs are mainly electrons [e.g., *McDiarmid et al.*, 1979; *Klumpar*, 1979; *Bythrow et al.*, 1982; *Sugiura et al.*, 1984; *Yamauchi et al.*, 1998]. The observed FAC temporal features are clearly associated with dynamic variations of their charge carriers, as they respond to variations of the electric field. The temporal time scales for the mesoscale FACs imply the same time scales for electric field temporal stability and variations. Among various sources of temporal variations, observations of parallel electric fields in the auroral acceleration show that their temporal variations have a time scale in the order of a few minutes, and thus are most likely to be the source of temporal variations of mesoscale FACs. Strong parallel electric fields have been observed or inferred in both upward and downward FAC regions by in situ measurements from satellites and sounding rockets [e.g., *Mozer and Kletzing*, 1998; *Ergun et al.*, 2000; *Andersson et al.*, 2002]. Observations have also suggested the similar time scales of a few minutes for their temporal variations. For example, on the basis of FAST single-spacecraft observations, *Ergun et al.* [1998] have suggested that the parallel electric field is stable on time scales of tens of seconds and over distances of tens to hundreds of kilometers. From Cluster multipoint observations, *Marklund et al.* [2001] have determined that the time scales for setting up the auroral parallel electric field (as they grow in magnitude and width) are in the order of ~2–5 min. In another example, *Marklund et al.* [2006] report that the time scale for the parallel electric field intensification is on a time scale of ~100–200 s. *Boudouridis and Spence* [2007] studied the spatial and temporal structure of auroral particle precipitation using data from conjunctions of two DMSP satellites. They found that for auroral features with scale lengths larger than ~100 km, their time scales for temporal stability are in the order of a few minutes, similar to our observations of mesoscale FACs. All these observations on the temporal stability of auroral

features have revealed the similar time scales as in our FAC observations.

[39] The most important contribution of the ST5 data to understanding dynamics of field-aligned currents is that they allow us for the first time to separate temporal and spatial structures and to evaluate their temporal variability in time scale ~10 min or less. Despite the fact that ST5 have provided first multipoint measurements of the magnetic field in low-altitude FAC region, and the unique data set enables us to determine the FAC properties more accurately, we need to acknowledge that the method we use to estimate the current density only makes incremental improvement that of single-spacecraft observations. Because of its string-of-pearls constellation configuration, we are not able to use the true curlmeter technique such as the one developed for Cluster data to calculate the current density [*Dunlop et al.*, 2002]. For some cases when two ST5 spacecraft are close enough to remain in the FAC region simultaneously, we were able to determine the current density using the gradiometer method which has the advantage of rejecting aliasing due to temporal variations [*Slavin et al.*, 2008]. The method we use in the paper is similar to the traditional technique-based single-spacecraft data except for some incremental improvements. First, we have corrected the spacecraft velocity relative to FAC current sheet by considering both the spacecraft and FAC motions, i.e., the assumption of stationary current sheet is no longer needed. We note that this correction is very small at low altitudes, typically less than 10%. But the correction will become very important at midaltitudes and high altitudes as the spacecraft motion becomes slower but FAC motion faster [*Wang et al.*, 2009]. Second, we use the Minimum Variance Analysis method to determine the current sheet orientation. Similar to the traditional single-spacecraft method, we still need to make the infinite current sheet assumption. But the MVA method determines the orientation of the infinite current sheet more accurately, and minimizes errors in the density of large-scale currents. Finally, we do not ignore the magnetic field variations in the direction along the FAC current sheet normal (δB_j) in determine the curl of the magnetic field since the magnetic field variations associated with mesoscale currents are very evident in the data. It reduces the errors in determine the current density associated with mesoscale currents.

4. Conclusions

[40] We have presented an event study of multipoint magnetic field measurements of field-aligned currents during and after a geomagnetic storm at low altitudes from ST5 constellation. The data show that mesoscale current structures, commonly observed embedded within large-scale field-aligned current sheets, are very dynamic with highly variable current density and/or polarity in time scales of ~10 min during the active period. They exhibit large temporal variations in such time scales during both quiet and disturbed times. On the other hand, they appear to be relatively stable in time scales of ~1 min. These temporal features are very likely associated with dynamic variations of their charge carriers (mainly electrons) as they respond to the variations of the parallel electric field in auroral acceleration region. The characteristic time scales for the temporal variability of mesoscale field-aligned currents are found to be consistent with those of auroral parallel electric field.

[41] **Acknowledgments.** We would like to thank the all the people whose commitment of time and professional expertise have made the ST5 project a success. The Wind solar wind and IMF data and the *Kp* index used in this study are extracted from the CDAWeb and OMNIWeb, respectively. The *Dst* index is calculated at Kyoto University.

[42] Zuyin Pu thanks the reviewers for their assistance in evaluating this paper.

References

Andersson, L., R. E. Ergun, D. Newman, J. P. McFadden, C. W. Carlson, and Y.-J. Su (2002), Characteristics of parallel electric fields in the downward current region, *Phys. Plasmas*, *9*, 3600–3609, doi:10.1063/1.1490134.

Boudouridis, A., and H. E. Spence (2007), Separation of spatial and temporal structure of auroral particle precipitation, *J. Geophys. Res.*, *112*, A12217, doi:10.1029/2007JA012591.

Buonsanto, M. J. (1999), Ionospheric storms—A review, *Space Sci. Rev.*, *88*, 563–601, doi:10.1023/A:1005107532631.

Bythrow, P. E., T. A. Potemra, and R. A. Hoffman (1982), Observations of field-aligned currents, particles, and plasma drift in the polar cusps near solstice, *J. Geophys. Res.*, *87*, 5131–5139, doi:10.1029/JA087iA07p05131.

Cargill, P. J., M. W. Dunlop, and A. Balogh (2001), First Cluster results of the magnetic field structure of the mid- and high-altitude cusps, *Ann. Geophys.*, *19*, 1533–1543.

Chappell, C. R., T. E. Moore, and J. H. Waite Jr. (1987), The ionosphere as a fully adequate source of plasma for the Earth's magnetosphere, *J. Geophys. Res.*, *92*, 5896–5910, doi:10.1029/JA092iA06p05896.

Chun, F. K., and C. T. Russell (1991), The evolution of field-aligned currents as a function of substorm phase, *J. Geophys. Res.*, *96*, 15,801–15,810, doi:10.1029/91JA01018.

Cowley, S. W. H. (1984), Solar wind control of magnetospheric convection, in *Achievements of the International Magnetospheric Study, IMS*, *Eur. Space Agency Spec. Publ., ESA SP-217*, 483–494.

Crowley, G., and C. Hackert (2001), Quantification of high latitude electric field variability, *Geophys. Res. Lett.*, *28*(14), 2783–2786, doi:10.1029/2000GL012624.

Draper, N. C., et al. (2005), Cluster magnetotail observations of a tailward-travelling plasmoid at substorm expansion phase onset and field-aligned currents in the plasma sheet boundary layer, *Ann. Geophys.*, *23*, 3667–3683.

Dunlop, M. W., A. Balogh, K.-H. Glassmeier, and P. Robert (2002), Four-point Cluster application of magnetic field analysis tools: The Curlometer, *J. Geophys. Res.*, *107*(A11), 1384, doi:10.1029/2001JA005088.

Emery, B. A., C. Lathuillere, P. G. Richards, R. G. Roble, M. J. Buonsanto, D. J. Knipp, P. Wilkinson, D. P. Sipler, and R. Niciejewski (1999), Time dependent thermospheric neutral response to the 2–11 November 1993 storm period, *J. Atmos. Sol. Terr. Phys.*, *61*, 329–350, doi:10.1016/S1364-6826(98)00137-0.

Ergun, R. E., et al. (1998), FAST satellite observations of electric field structures in the auroral zone, *Geophys. Res. Lett.*, *25*, 2025–2028, doi:10.1029/98GL00635.

Ergun, R. E., C. W. Carlson, J. P. McFadden, F. S. Mozer, and R. J. Strangeway (2000), Parallel electric fields in discrete arcs, *Geophys. Res. Lett.*, *27*, 4053–4056, doi:10.1029/2000GL003819.

Erlandson, R. E., L. J. Zanetti, T. A. Potemra, and P. F. Bythrow (1988), IMF By dependence of region 1 Birkeland currents near noon, *J. Geophys. Res.*, *93*, 9804–9814, doi:10.1029/JA093iA09p09804.

Figueiredo, S., G. T. Marklund, T. Karlsson, T. Johansson, Y. Ebihara, M. Fjiri, N. Ivchenko, P.-A. Lindqvist, H. Nilsson, and A. Fazakerley (2005), Temporal and spatial evolution of discrete auroral arcs as seen by Cluster, *Ann. Geophys.*, *23*, 2531–2557.

Fukunishi, H., R. Fujii, S. Kokubun, F. Tohyama, T. Mukai, and H. Oya (1991), Small-scale field-aligned currents observed by the Akebono (EXOS-D) satellite, *Geophys. Res. Lett.*, *18*(2), 297–300, doi:10.1029/91GL00036.

Fung, S., and R. Hoffman (1992), Finite geometry effects of field-aligned currents, *J. Geophys. Res.*, *97*(A6), 8569–8579, doi:10.1029/91JA03026.

Higuchi, T., and S. Ohtani (2000), Automatic identification of large-scale field-aligned current structures, *J. Geophys. Res.*, *105*(A11), 25,305–25,315, doi:10.1029/2000JA900073.

Hoffman, R. A., M. Sugiura, and N. C. Maynard (1985), Current carriers for the field-aligned current system, *Adv. Space Res.*, *5*, 109–126, doi:10.1016/0273-1177(85)90124-3.

Hoffman, R. A., R. Fujii, and M. Sugiura (1994), Characteristics of the field-aligned current system in the nighttime sector during auroral substorms, *J. Geophys. Res.*, *99*(A11), 21,303–21,325, doi:10.1029/94JA01659.

Iijima, T., and T. A. Potemra (1978), Large-scale characteristics of field-aligned currents associated with substorms, *J. Geophys. Res.*, *83*, 599–615, doi:10.1029/JA083iA02p00599.

Johansson, T., S. Figueiredo, T. Karlsson, G. Marklund, A. Fazakerley, S. Buchert, P.-A. Lindqvist, and H. Nilsson (2004), Intense high-altitude auroral electric fields—Temporal and spatial characteristics, *Ann. Geophys.*, *22*, 2485–2495.

Kelly, T., C. Russell, R. Walker, G. Parks, and J. Gosling (1986), ISEE 1 and 2 observations of Birkeland currents in the Earth's inner magnetosphere, *J. Geophys. Res.*, *91*(A6), 6945–6958, doi:10.1029/JA091iA06p06945.

Klumpar, D. M. (1979), Relationships between auroral particle distributions and magnetic perturbations associated with field-aligned currents, *J. Geophys. Res.*, *84*, 6524–6532, doi:10.1029/JA084iA11p06524.

Lockwood, M., S. E. Milan, T. Onsager, C. H. Perry, J. A. Scudder, C. T. Russell, and M. Brittnacher (2001), Cusp ion steps, field-aligned currents and poleward moving auroral forms, *J. Geophys. Res.*, *106*(A12), 29,555–29,569, doi:10.1029/2000JA900175.

Marchaudon, A., J.-C. Cerisier, O. Amm, M. Lester, C. W. Carlson, and G. K. Parks (2004), Quantitative modelling of the closure of meso-scale parallel currents in the nightside ionosphere, *Ann. Geophys.*, *22*, 125–140.

Marklund, G. T., et al. (2001), Temporal evolution of the electric field accelerating electrons away from the auroral ionosphere, *Nature*, *414*, 724–727, doi:10.1038/414724a.

Marklund, G. T., T. Karlsson, S. Figueiredo, T. Johansson, P.-A. Lindqvist, M. André, S. Buchert, and L. M. Kistler (2006), Dynamics and characteristics of electric-field structures in the auroral return current region observed by Cluster, *Phys. Scr. T*, *122*, 34–43, doi:10.1088/0031-8949/2006/T122/008.

McDiarmid, I. B., J. R. Burrows, and M. D. Wilson (1979), Large-scale magnetic field perturbations and particle measurements at 1400 km on the dayside, *J. Geophys. Res.*, *84*, 1431–1441, doi:10.1029/JA084iA04p01431.

McPherron, R. L., C. T. Russell, and M. Aubry (1973), Satellite studies of magnetospheric substorms on August 15, 1978: 9. Phenomenological model for substorms, *J. Geophys. Res.*, *78*, 3131–3149, doi:10.1029/JA078i016p03131.

Moore, T. E. (1991), Origins of magnetospheric plasma, *U.S. Natl. Rep. Int. Union Geod. Geophys. 1987–1990*, *Rev. Geophys.*, *29*, 1039–1048.

Mozer, F. S., and C. A. Kletzing (1998), Direct observation of large, quasi-static, parallel electric fields in the auroral acceleration region, *Geophys. Res. Lett.*, *25*, 1629–1632, doi:10.1029/98GL00849.

Neubert, T., and F. Christiansen (2003), Small-scale, field-aligned currents at the top-side ionosphere, *Geophys. Res. Lett.*, *30*(19), 2010, doi:10.1029/2003GL017808.

Slavin, J. A., G. Le, R. J. Strangeway, Y. Wang, S. A. Boardsen, M. B. Moldwin, and H. E. Spence (2008), Space Technology 5 multi-point measurements of near-Earth magnetic fields: Initial results, *Geophys. Res. Lett.*, *35*, L02107, doi:10.1029/2007GL031728.

Sonnerup, B. U. Ö., and L. J. Cahill Jr. (1967), Magnetopause structure and attitude from Explorer 12 observations, *J. Geophys. Res.*, *72*, 171–183, doi:10.1029/JZ072i001p00171.

Sugiura, M., T. Iyemori, R. A. Hoffman, N. C. Maynard, J. L. Burch, and J. D. Winningham (1984), Relationships between field-aligned currents, electric fields, and particle precipitation as observed by Dynamic Explorer-2, in *Magnetospheric Currents*, *Geophys. Monogr. Ser.*, vol. 28, edited by T. A. Potemra, pp. 96–103, AGU, Washington, D. C.

Wang, Y., G. Le, J. A. Slavin, S. A. Boardsen, and R. J. Strangeway (2009), Space Technology 5 measurements of auroral field-aligned current sheet motion, *Geophys. Res. Lett.*, *36*, L02105, doi:10.1029/2008GL035986.

Yamauchi, M., R. Lundin, L. Eliasson, S. Ohtani, and J. H. Clemmons (1998), Relationships between large-, meso-, and small-scale field-aligned currents and their current carriers, in *Polar Cap Boundary Phenomena*, edited by J. Moen et al., pp. 173–188, Kluwer Acad., Dordrecht, Netherlands.

G. Le, Space Weather Laboratory, Heliophysics Science Division, NASA Goddard Space Flight Center, Code 674, Greenbelt, MD 20771, USA. (guan.le@nasa.gov)

J. A. Slavin, Heliophysics Science Division, NASA Goddard Space Flight Center, Code 670, Greenbelt, MD 20771, USA. (james.a.slavin@nasa.gov)

R. J. Strangeway, Institute of Geophysics and Planetary Physics, University of California, Los Angeles, CA 90095-1567, USA. (strange@igpp.ucla.edu)

Y. Wang, UMBC/GEST at Space Weather Laboratory, NASA Goddard Space Flight Center, Code 674, Greenbelt, MD 20771, USA. (yongli.wang@nasa.gov)